On the occurrence and spatial extent of electron precipitation induced by oblique nonducted whistler waves

W. B. Peter and U. S. Inan

Space Telecommunications and Radioscience Laboratory, Stanford University, Stanford, California, USA

Received 30 January 2004; revised 23 June 2004; accepted 10 September 2004; published 18 December 2004.

[1] Two different 4-hour sequences of subionospheric Very Low Frequency (VLF) signal perturbations are examined to characterize electron precipitation induced by nonducted obliquely propagating whistlers. These lightning-induced electron precipitation (LEP) events are typically associated with cloud-to-ground lightning discharges. The temporal and spatial signatures of LEP events associated with two disparate storms occurring over two 4-hour periods are examined. A distributed set of VLF observing sites, known as the Holographic Array for Ionospheric and Lightning Research (HAIL), captures the full latitudinal extent of the events, providing evidence that 90% of the precipitation occurs over a region 8° ± 1° and 9° ± 1° in latitudinal extent for the two time periods. The measured peak of the precipitation is poleward displaced (6°45′ ± 30′ and 7°45′ ± 30′ for the two case studies) from the causative discharge. Analysis indicates that the onset delay and the duration of precipitation steadily increase with increasing *L*-value, while the signal recovery time is independent of *L*-value for the LEP events associated with both storms. The causative lightning discharges associated with the two storms were located at different latitudes. For lightning occurring in the storm at higher latitudes, the associated LEP events are of longer duration and exhibit precipitation in a smaller area displaced less from the causative discharge. The onset delays and event durations increase more rapidly with increasing *L*-value for events associated with lightning occurring in the storm at higher latitudes. The general spatial and temporal signatures are consistent with those expected for LEP events induced by nonducted whistlers. *INDEX TERMS:* 2455 Ionosphere: Particle precipitation; 2716 Magnetospheric Physics: Energetic particles, precipitating; 2431 Ionosphere: Ionosphere/magnetosphere interactions (2736); 7867 Space Plasma Physics: Wave/particle interactions; *KEYWORDS:* nonducted, precipitation, whistlers

Citation: Peter, W. B., and U. S. Inan (2004), On the occurrence and spatial extent of electron precipitation induced by oblique nonducted whistler waves, *J. Geophys. Res.*, *109*, A12215, doi:10.1029/2004JA010412.

1. Introduction

[2] Subionospheric Very Low Frequency (VLF) signals have long been used to detect transient perturbations of the upper atmosphere associated with lightning-induced electron precipitation (LEP) events [e.g., *Helliwell et al.*, 1973; *Inan et al.*, 1985; *Inan and Carpenter*, 1986; *Inan et al.*, 1988a]. Early work [e.g., *Burgess and Inan*, 1993, and references therein] regarding LEP events focused on precipitation which was believed to be induced by "ducted" whistler waves propagating along field-aligned ducts of enhanced ionization. More recent work [e.g., *Johnson et al.*, 1999] has demonstrated that precipitation of energetic electrons can be caused by obliquely propagating "nonducted" whistlers, in a manner consistent with predictions of a quantitative model [*Lauben et al.*, 2001]. However, the temporal and spatial characteristics of these events have not yet been quantified experimentally. In this paper, we present new data on the occurrence rates of nonducted LEP events and the spatial extent of the associated precipitation regions.

[3] Lightning is pervasive around our planet, with on the average ~40 lightning discharges occurring every second [*Christian et al.*, 1999]. Both theoretical [*Bortnik et al.*, 2003; *Abel and Thorne*, 1998a, 1998b] and experimental works [e.g., *Burgess and Inan*, 1993; *Voss et al.*, 1998] suggest that wave energy injected by lightning discharges may be an important contributor to the loss rates of radiation belt particles, especially at lower *L*-shells ($L < 3$). Having a better understanding of the occurrence properties and spatial extent of nonducted LEP events can enable us to be more accurate in quantifying the role of lightning discharges in radiation belt losses.

[4] VLF waves are guided within the spherical waveguide formed between the Earth and the ionosphere (Figure 1b). The amplitude and phase of the subionospherically propa-

0148-0227/04/2004JA010412$09.00

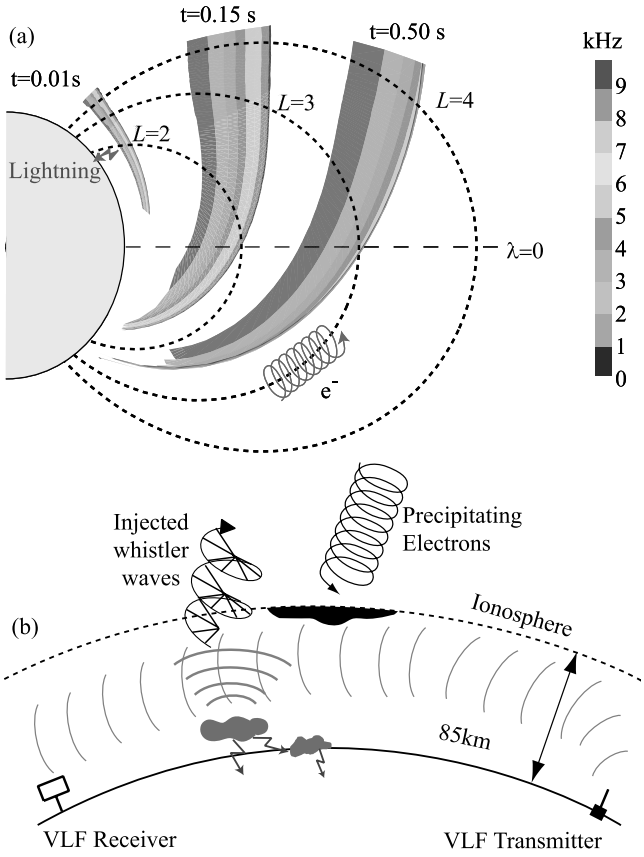

Figure 1. Electron precipitation induced by obliquely propagating (nonducted) whistlers. (a) A lightning discharge emits VLF wave energy, a portion of which is coupled into the magnetosphere and propagates therein as an oblique whistler wave. Wave-particle interaction near the equatorial plane scatters a fraction of the trapped energetic radiation belt electrons into the loss cone, causing them to precipitate and produce secondary ionization (b), which in turn changes the electrical conductivity of the upper boundary of the Earth-ionosphere waveguide and perturbs the VLF wave propagating underneath.

gating VLF signals depend sensitively on the electrical conductivity of the lower ionosphere as well as that of the ground. The amplitude and phase of VLF transmitter signals observed at any point can thus be used to measure the spatial and temporal structure of localized disturbances in the lower ionosphere that overlie, or are near, the great circle paths (GCPs) between the transmitter and the receiver(s).

[5] Lightning discharges indirectly produce localized ionospheric disturbances as a result of lightning-induced precipitation of bursts of energetic radiation belt electrons. Lightning-induced Electron Precipitation (LEP) events are produced by the fraction of the VLF energy radiated by lightning discharges that escapes into the magnetosphere and propagates as a whistler-mode wave (Figure 1a). The whistler-mode wave interacts with trapped radiation belt electrons through cyclotron resonant pitch angle scattering, causing some of those close to the loss cone to precipitate and produce secondary ionization. In nonducted LEP events, the whistler wave energy that leaks upward through the ionosphere enters the magnetosphere and propagates in the so-called nonducted mode, with the **k** vector not being constrained to a narrow cone of angles around the direction of the static magnetic field. In this type of oblique whistler-wave propagation, wave energy tends to migrate across the magnetic field lines from initially lower L-shells to higher L-shells [*Lauben et al.*, 2001]. The scattering caused by obliquely propagating whistlers thus leads to precipitation over an extended region of the upper atmosphere, with a continuum of onset delays (with respect to the time of the lightning source) and of event durations as a function of latitude [*Lauben et al.*, 1999].

[6] Precipitating energetic electrons ($\sim$50 to 500 keV) cause secondary ionization via impact with atmospheric constituents, altering the conductivity of the D region of the ionosphere. This ionospheric disturbance in turn changes the amplitude and/or phase of VLF transmitter signals propagating in the Earth-ionosphere waveguide on great circle paths that pass through or near the localized disturbances [*Poulsen et al.*, 1993b]. The fact that resulting ionospheric disturbances decay away (via recombination and/or attachment) over 10–100 s allows ample time to detect LEP events by means of the associated VLF signal perturbations, which can be measured with high enough time resolution to delineate temporal features such as onset delay (the time between the causative lightning discharge and the onset of the event) and event duration (the time over which the signal amplitude continues to change). The use of multiple synchronous VLF measurements yields information about the temporal and spatial characteristics of the lightning-induced electron precipitation [*Inan and Rodriguez*, 1993].

[7] In contrast to ducted whistler-induced electron precipitation, in which the precipitation signatures do not exhibit a pronounced dependence on the location of the causative discharge [*Inan et al.*, 1988a], it has been shown theoretically [*Lauben et al.*, 1999, 2001] that for nonducted whistler-induced electron precipitation the location of the causative discharge strongly influences the temporal signatures and spatial distribution of the induced precipitation. Lightning sources at higher latitudes produce stronger whistler intensities at higher L-shells, which combine with the generally longer interaction lengths (the distance over which the conditions for gyroresonance between the whistler wave mode and the energetic electrons are satisfied) at these field lines to markedly increase the precipitated flux intensity, spatial extent and duration of the precipitation. The location of the causative discharge strongly influences the temporal and spatial signatures of LEP events. As an example, *Lauben et al.* [2001] predicted, for a lightning source latitude of 19°N (geographic), that the separation between the lightning discharge and the location of the peak electron precipitation would be $\sim$20°, while for a higher source latitude of 29°N the separation would diminish to $\sim$12°, owing to the tighter field line convergence at higher L-shells. In this paper, we examine the variations in the temporal signatures and the spatial extent of LEP events for two separate storms of different latitudes, albeit with a smaller difference in the location of lightning flashes (a mean difference of 3.8° of latitude) than that modeled in theoretical work [*Lauben et al.*, 2001].

[8] Both of the thunderstorms considered in our statistical analysis contain lightning discharges that induce detectable electron precipitation events that exhibit differential delay patterns consistent with precipitation induced by nonducted whistler waves. Analysis of the high resolution VLF data allows us to quantify several parameters of nonducted whistler-induced precipitation events. Measurements of the onset delay between the causative lightning discharge and the first appearance at the ionosphere of the bursts of electrons precipitated on different field lines show a steadily increasing onset delay with increasing L-value, which has previously been used as the delineating signature of nonducted LEP events [*Johnson et al.*, 1999]. In this paper, we show that the dependence of the onset delay on the distance from the causative discharge for LEP events associated with lightning in both storms agrees with previous measurements presented in *Johnson et al.* [1999]. We also show that the onset delays for LEP events associated with lightning flashes occurring in the two storms of different location are measurably different in a manner consistent with theoretical predictions [*Lauben et al.*, 2001]. Our analysis additionally allows the assessment of the full spatial extent (in latitude) of the disturbed ionospheric region and the dependence of the magnitude of the VLF perturbation on the distance between the propagating VLF wave and the location of the causative discharge. The precipitation region is shown to be poleward-displaced in geomagnetic latitude with respect to the causative lightning flash, with the VLF perturbation magnitude (and thus presumably the precipitation flux) having an approximately Gaussian profile in latitude with 90% of the precipitation typically occurring over a region with spatial extents of 880 ± 110 km and 990 ± 110 km respectively for the two cases studied. Differences in the spatial extent and poleward-displacement of the disturbed ionospheric region are found to be discernable for lightning discharges associated with the two different storm locations. We also measure the duration of nonducted LEP events and measure variations in the event duration with distance of the subionospheric VLF Great Circle Path from the location of the causative discharge. The event durations also differ for the LEP events associated with lightning occurring in the two different storm locations, once again in a manner consistent with theoretical predictions. Our results additionally indicate a distinct positive correlation between the peak current of cloud-to-ground (CG) lightning discharges and the percent of flashes associated with nonducted LEP events.

[9] In general, our results are consistent with the predictions of previous theoretical work [*Lauben et al.*, 1999], and provide a preliminary quantitative basis for assessing the contribution of the LEP process to the loss of radiation belt particles on a global scale, since most of the wave energy launched into the magnetosphere propagates in the nonducted mode [*Bortnik et al.*, 2003].

2. Description of Experiment

[10] The Holographic Array for Ionospheric/Lightning research (HAIL) consists of thirteen separate VLF receivers spaced ~65 km apart along the "Front Range" of the Rocky Mountains. The HAIL array continuously monitors the amplitude and phase of coherent and subionospherically propagating VLF transmitter signals produced by the United States Navy in Washington (NLK at 24.8 kHz), Maine (NAA at 24.0 kHz), Hawaii (NPM at 21.4 kHz) and Puerto Rico (NAU at 40.75 kHz). This study focuses on the recorded data for the month of March 2001, from only the NAA and NAU transmitters.

Table 1. Measurables of LEP Events

Measurable	Qualification
Perturbation magnitude	$\Delta A \geq 0.5$
Onset delay	200 ms $\leq \Delta t \leq 2.5s$
Event duration	$0.5s \leq t_d \leq 5s$
Recovery time	$10s \leq t_r \leq 100s$

[11] Data are typically acquired everyday from 01:00 to 13:00 UT, when the great circle paths (GCPs) between transmitter and receiver are partially or wholly in the nighttime sector. A 1.7 × 1.7 m^2 magnetic loop antenna connected to a preamplifier is used to detect the VLF signal at all receivers. The broadband VLF signal is bandpass filtered to a range of 9–45 kHz and then is digitized at a rate of 100 kHz with 16-bit resolution, with triggers provided by GPS timing. Each receiver digitally down-converts the individual VLF transmitter signals and records the demodulated amplitude and phase with 20 ms resolution. Only amplitude data is included in this study, both because sferic noise typically requires a longer averaging period for phase measurements and because our conclusions are sufficiently drawn from the relative magnitudes of VLF signal changes observed at different sites. The National Lightning Detection Network (NLDN) provides the timing, location and peak current of the cloud-to-ground (CG) lightning discharges with one-ms resolution [*Cummins et al.*, 1998]. These data were used to locate the causative lightning discharges for the LEP events for the two days of the study.

[12] Subionospheric VLF signatures of LEP events occur when whistler waves originating in lightning discharges cause the precipitation of bursts of energetic electrons onto atmospheric regions that are near the VLF GCPs (Figure 2a), producing changes in the electrical conductivity of the D region at altitudes below the nighttime VLF reflection height (~85 km) and thus perturbing the amplitude and/or phase of the VLF signals propagating in the Earth-ionosphere waveguide. In typical events, the measurable features (Table 1) of VLF signal perturbations consist of the following:

[13] 1. Event perturbation magnitude (ΔA) of the VLF signal refers to the change in amplitude, measured in dB, from the ambient levels prior to the event, to the maximum (or minimum) levels reached during the event (Figure 2c). The associated phase change $\Delta\phi$ is also measured, but not used in this particular study.

[14] 2. Onset delay (Δt) refers to the time between the causative lightning discharge, as recorded in NLDN data and time-correlated to sferics in the HAIL VLF data, and to the onset of the event (Figure 2c). The impulsive sferic associated with the lightning discharge contains energy over a wide range of frequencies and is often visible as a sharp peak in many of the narrowband channels monitored. For

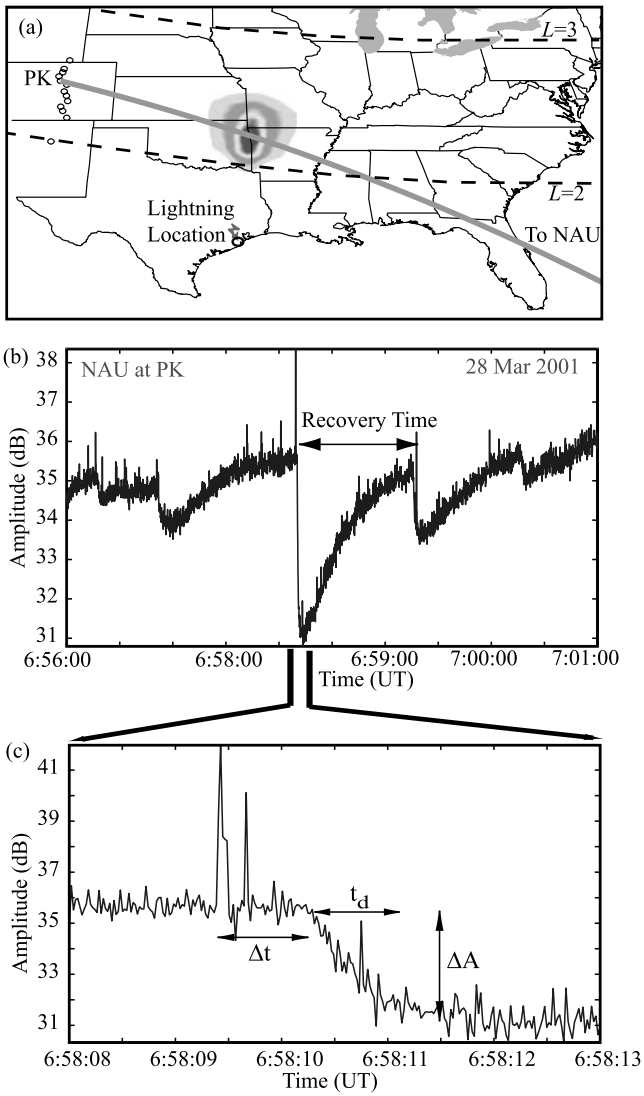

Figure 2. An example LEP event (~6:58:09). (a) Great circle path (GCP) of the subionospherically propagating VLF wave, with the presumed precipitation region superimposed. The change in the conductivity of the *D* region of the ionosphere leads to the perturbation of the VLF signal propagating underneath. (b) A 5-min snapshot of the received VLF signal for a typical LEP event, showing one of the measurable temporal features, namely, the recovery time. The panel shows the amplitude of the received signal in dB. (c) A zoom-in of the same event showing a 5-s snapshot, which shows the other three measurable temporal features, namely, event perturbation magnitude (ΔA), onset delay (Δt), and event duration (t_d).

the purposes of this study, the onset of the event is defined as the time at which the amplitude has changed by 10% of the final perturbation magnitude (ΔA). With the onset time defined in this manner, the onset delay measurement is relatively independent of the magnitude of the perturbation.

[15] 3. Event duration (t_d) refers to the length of time over which the signal amplitude continues to change up to its maximum value (either negative or positive), and corresponds to the temporal duration of the precipitation burst (Figure 2c). The event duration is defined as the time between the onset of the event and the end of the event, the latter being defined as the point at which the signal amplitude change has reached 90% of its full value (ΔA). The measurement of the event duration is also relatively independent of the magnitude of the perturbation.

[16] 4. Recovery time (t_r) is the time at which the signal recovers back to the amplitude it would have exhibited in the absence of the perturbation, and it signifies the time at which the ionosphere recovers back to its ambient profile (Figure 2b). For the purposes of this paper, recovery time is defined as the time between the time of maximum perturbation and the time when the amplitude has returned to within 10% of the value it would have had in the absence of the event, so that it also is relatively independent of the magnitude of the perturbation. If the recovery is interrupted by another event, it is assumed that the event would have recovered at a similar rate, and the typically exponential recovery of the signal is extrapolated to estimate the recovery time.

[17] Typical VLF signatures associated with nonducted whistler-induced electron precipitation exhibit an increase in onset delay with latitude [*Johnson et al.*, 1999]. Figure 3 shows a LEP event recorded at several receivers. The signals arriving over the corresponding GCPs exhibit the event onset at increasingly later times with increasing latitude of the GCP. The differences in onset delay across the receiver sites at which the event is visible are referred to as "differential onset delay." This difference in onset delays is the temporal signature that distinguishes the so-called nonducted LEP events produced by an obliquely propagating (nonducted) whistler from other events such as those produced by ducted whistlers.

[18] During March 2001, an unusually large number of LEP events were captured by the HAIL array. While the signal amplitudes exhibited significant variations over various time scales, the VLF signatures of LEP events were identified on the basis of previously established criteria [*Johnson et al.*, 1999], including a rapid event duration (0.5 to 5 s) followed by a slower recovery (10 to 100 s). The onset delay itself was found to vary significantly, depending on the geomagnetic latitude of the GCP of the perturbed VLF signal. The onset delay was required to be greater than 0.2 s to ensure that other VLF events, known as Early/Fast events [*Inan et al.*, 1995], were not included in the data set. For the purposes of this paper, only those with perturbation magnitudes larger than 0.5 dB were considered, for ease of identification and accuracy in the presence of other fluctuations in signal amplitude. While our choice of a threshold of 0.5 dB excluded smaller LEP events from the study, it allows for a more reliable measurement of the different temporal features for the events included in our study. In this context, it should be noted that both the duration and recovery time measurables required measurement changes of 10% of the perturbation magnitude, or a minimum of 0.05 dB; only slightly larger than the inherent ambient noise on the recorded signal amplitudes.

3. VLF Signatures of LEP Events Observed During March 2001

[19] Data from the HAIL array were collected during the entire month of March 2001, with at least five receivers

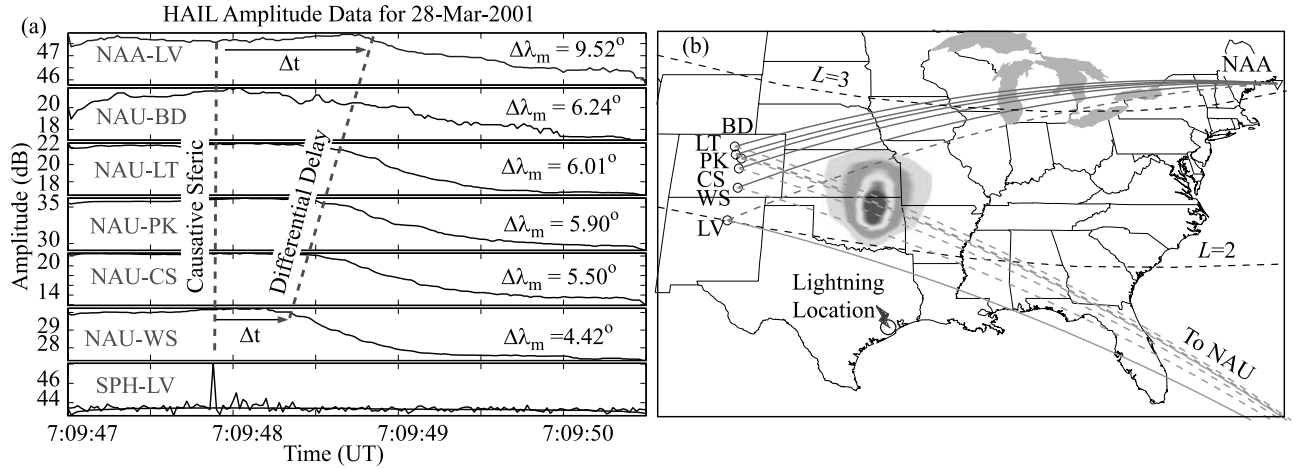

Figure 3. An example LEP event (~7:09:48) shows a differential onset delay as measured on the different VLF paths spanning the HAIL array. (a) A 3.5-s snapshot of each of the perturbed signals, shown in amplitude (dB). The distance ($\Delta\lambda_m$), in degrees latitude, between the flash location (30°11′N, 95°44′W) and the point of crossing of the GCP of the geomagnectic longitude of the causative flash is shown for each signal. (b) The perturbed great circle paths (GCPs) of propagating VLF waves, with the presumed precipitation region. The dashed lines denote those GCPs the signals propagating on which are disturbed, while no measurable perturbations were detected on the signals propagating along the paths denoted by solid lines. The increase in onset delay with latitude is termed "differential delay."

operating on each day of the month. The recorded signals (from NAA and NAU) for each day were examined for VLF signatures of LEP events that met the criteria specified above. The number of LEP events on each day of March 2001 is shown in Figure 4c. Only those events with perturbation magnitudes greater than 0.5 dB were considered as LEP events in this study, irrespective of perturbations on a smaller scale that might have been associated with lightning induced nonducted whistlers. As the occurrence of lightning discharges is a prerequisite for lightning-induced electron precipitation, Figure 4b shows the number of lightning strikes occurring in the region typically associated with producing LEP events detectable on the HAIL array, as denoted by the boxed region in Figure 4a. Due to the poleward displacement of the precipitation region from the causative discharge, the boxed area includes areas distant from the GCPs of the propagating VLF signals. The exact dimensions of the region were chosen based on our familiarity with HAIL data and the knowledge of which regions of lightning activity typically result in producing LEP events detectable on the HAIL array. Possible reasons for the small numbers of LEP events compared to the number of CG discharges recorded by the NLDN network are discussed in section 4.1.

[20] The number of LEP events on any given day was found to be highly variable, with the latter days of the month tending to exhibit a higher number of occurrences of events (Figure 4c). The occurrence of a lower number of LEP events on the 26th and 27th corresponds to a period when few lightning discharges occurred in the boxed region. However, a relatively small number of LEP events occur on earlier days (the 12th, 13th, 15th and 16th) with a large number of lightning flashes. The lack of correlation between Figures 4b and 4c suggest that factors other than CG lightning frequency significantly influence the frequency of LEP events.

[21] The early part of the month was a period of relatively quiet geomagnetic conditions (as indicated by the K_p index shown in Figure 4d and the Dst shown in Figure 4e). Interestingly, many of the later days of the month, starting at about the 19th and 20th, correspond to a period of high geomagnetic activity with a high K_p index. It has been suggested that there is a relationship between geomagnetic activity and the conditions conducive to the occurrence of detectable LEP events [*Leyser et al.*, 1984]. The Dst index (Figure 4e) shows that energetic electron population in the ring current was highly variable during the later parts of the month. Therefore a possible explanation for the variance in LEP events detected in this study is that the energetic electron population in the slot region increased with the advent of geomagnetic activity. Such an enhancement in the population of energetic electrons available for scattering into the loss cone by lightning induced whistlers would proportionally increase the resulting precipitation fluxes, leading to the production of more frequent bursts of precipitation of sufficient magnitude to be classified as LEP events.

[22] Figure 5 shows NOAA-16 POES satellite data for six passes over the HAIL array during March 2001. Data are shown (Figure 5a) for the Space Environment Monitor's (SEM-2) Medium Energy Proton and Electron Detector (MEPED). The low altitude (830 to 870 km) polar-orbiting (98° inclination) satellite monitors the flux of energetic electrons. The data shown here are 16-s averaged 100–300 keV electron flux. For all passes, the angle of the detector with respect to the magnetic field remained nearly constant, between 60° and 70°. Furthermore, the variation of the angle with L-shell is nearly identical (±1°) for each pass. The detector's aperture has a 15° half-angle cone. It is assumed that these measurements are representative of the flux of energetic electrons available for pitch-angle scattering into the loss cone by nonducted whistler wave interac-

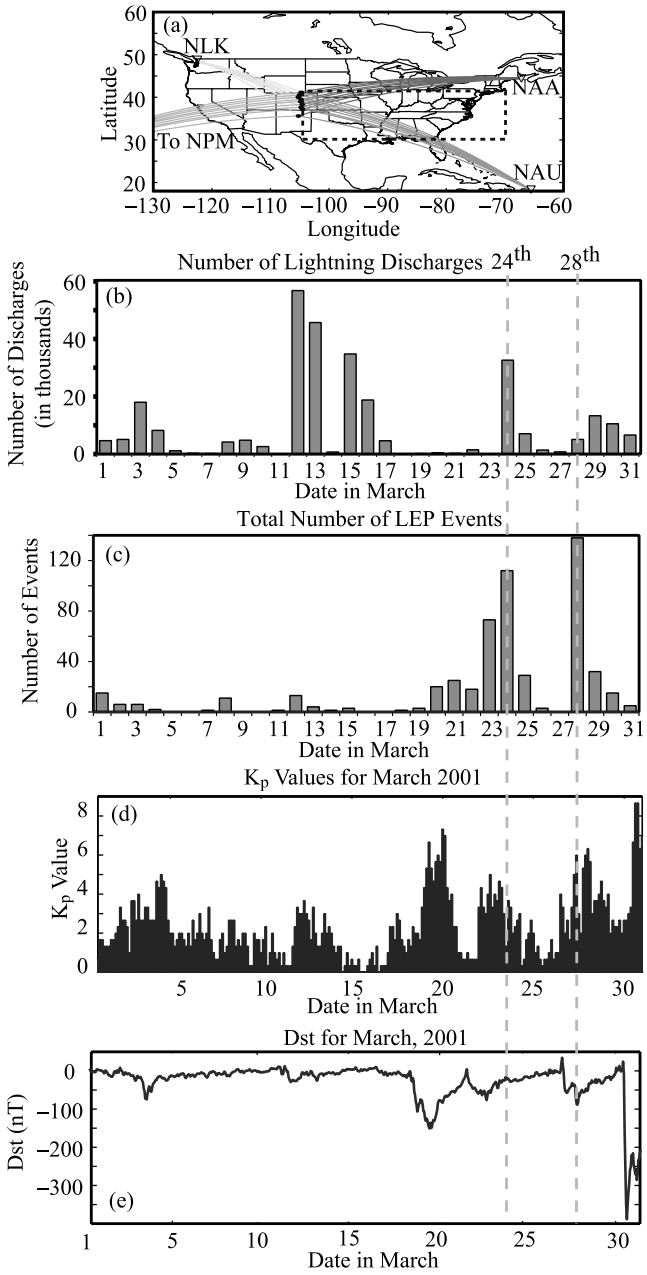

Figure 4. (b) The number of cloud-to-ground (CG) discharges recorded by NLDN from 1:00 to 13:00 UT on each day of March 2001, and occurring in that area (denoted by the boxed region shown on the map (a) from 30° to 42°N and −70° to −105°W), generally associated with producing LEP events monitored by the HAIL array. (c) The number of LEP events observed on each day of March 2001. (d) Geomagnetic activity (K_p) index for the month of March 2001. (e) Dst index for the month of March 2001.

tion. Since the angle (with respect to the magnetic field) of the detector is similar for each pass, the variations in flux observed for the different passes are not likely to be due to differences in the measurement angle. Figure 5b shows a map of the corresponding tracks of the satellite passes over the HAIL array, projected down to 120 km altitude along the field line passing through the satellite. All passes occurred during the night between 7:00 and 9:30 UT, with each pass taking less than 10 min to cross over the region of interest.

[23] During the early part of the month, when the occurrence rates of detected LEP events were low, the detected energetic electron flux levels were also lower (Figure 5a). The passes for both 2 and 15 March are representative of the low flux levels detected during the first half of the month. However, on 20 March, a sharp increase in flux levels is observed, with this trend continuing on to 21 March. This increase suggests that the energetic electron population in the slot region ($L = 2$ to 3) was enhanced by at least an order of magnitude above that observed earlier in the month. This time period corresponds to a period of high geomagnetic activity (Figures 4d and 4e) when the energetic electron population in the slot region has been shown to frequently increase [*Friedel and Korth*, 1995]. The high levels of flux continue throughout the rest of the month, including the 2 days of the case study (24 and 28 March). It is during this later part of the month when a relatively large number of LEP events are detected on the HAIL array. This occurrence supports the notion that the variance in the number of LEP events detected is largely due to the energetic electron population in the slot region increasing with the advent of geomagnetic activity, thus increasing the population of energetic electrons available for scattering into the loss cone by lightning induced whistlers.

[24] The data in Figures 4 and 5 are consistent with the previously noted [*Leyser et al.*, 1984] relations between geomagnetic activity and the conditions conducive to the occurrence of detectable LEP events. However, a significantly longer time epoch of analysis is necessary to accurately establish the degree of this correlation, especially since the variable occurrence of lightning activity is a necessary prerequisite for LEP events to occur. Further work is also needed to determine what other factors, besides geomagnetic conditions and CG lightning flash rates, might influence the frequency of LEP events.

[25] Furthermore, daily variations in the percentage of CG flashes that induce detected LEP events (Figures 4b and 4c) are likely a result of the different magnetospheric conditions causing variations in the flux of trapped electrons (Figure 5), since precipitation induced by discrete waves is proportional to the available trapped flux. Thus, the LEP activity as measured on the HAIL array may be a rudimentary indicator of magnetospheric conditions, or the trapped radiation flux levels.

[26] The peaks of LEP activity in March 2001 occurred on 24 and 28 March. The lightning storms that contained the causative lightning discharges on these two days are shown in Figure 6. The lightning storm on the 24 March was located in northern Texas, with over 34,000 cloud-to-ground (CG) flashes detected by the NLDN network from 6:00 to 10:00 UT. The storm remained quite localized, with little movement over this four-hour period. The mean location of all CG flashes recorded by NLDN for these four hours was at 32°57′N, 98°10′W, with a standard deviation in flash location of 58′ in latitude and 3°48′ in longitude. The storm on 28 March was located on the southeastern coast of Texas, with over 4,800 GC flashes detected by the NLDN network between 6:00 and 10:00 UT. This storm was also quite localized, with little movement

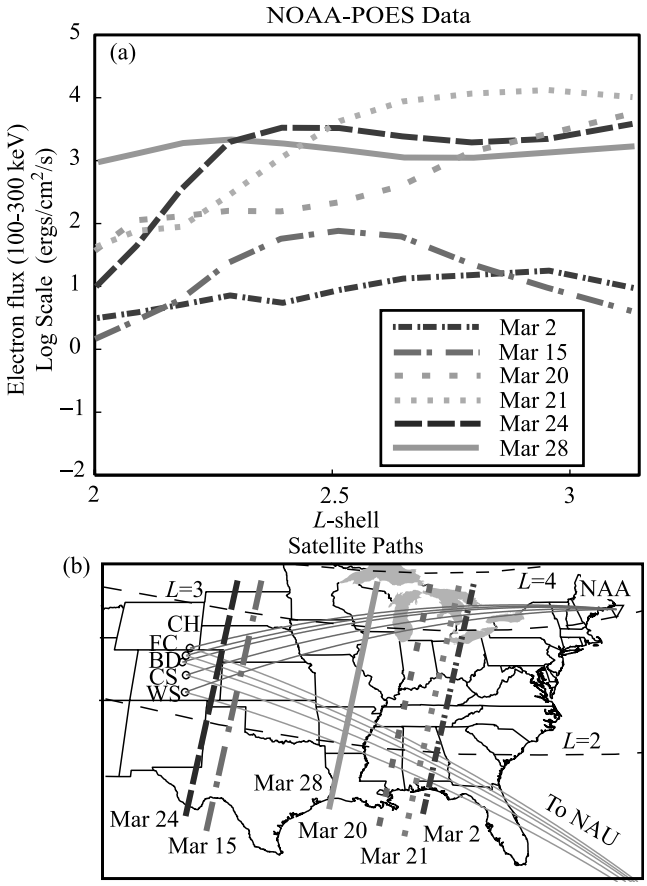

Figure 5. Energetic Electron Flux Data for March 2001. (a) Data from the Space Environment Monitor's (SEM-2) Medium Energy Proton and Electron Detector (MEPED) aboard the NOAA-16 POES satellite. The low altitude (830 to 870 km) polar-orbiting (98° inclination) satellite monitors the flux of energetic electrons. The data shown here is 16-s averaged 100–300 keV electron flux with the detector nearly perpendicular (with a window of 30°) to the magnetic field. (b) A map of the corresponding tracks of the satellite passes over the HAIL array, projected down to 120 km altitude along the field line passing through the satellite. All passes occurred during the night between 7:00 and 9:30 UT, with each pass taking less than 10 min over the region of interest.

over the four-hour period. The mean location of all CG flashes recorded by NLDN for these four hours was at 29°9′N, 95°11′W, with a standard deviation in flash location of 48′ in latitude and 2°5′ in longitude.

[27] Due to the 3°48′ difference in geographic latitude (3°37′ geomagnetic latitude) of the mean locations of the CG flashes detected by the NLDN network for the two storms, nonducted whistlers induced by lightning discharges associated with the different storms are expected to enter the magnetosphere at different *L*-shells, resulting in different precipitation signatures as a function of *L*-shell or geomagnetic latitude. Previous theoretical work [*Lauben et al.*, 1999] predicted the spatial distribution of the ionospheric "hot spots" (or precipitation regions) resulting from various locations of causative discharges, looking at differences of 10 degrees in latitude. The spatial and temporal distribution of the precipitation region was found to depend critically on the location of the causative discharges. The difference in source latitude in this study (∼4 degrees) is significantly smaller than that used in the model. It is assumed that this difference in source latitude would produce measurable differences (albeit on a smaller scale than in the theoretical work) in the precipitation signatures of LEP events for the two case studies. While it is unclear whether the differences observed in the precipitation signatures for the two time periods are due to this difference in latitude injection or due to other factors (i.e., geomagnetic activity, ionospheric conditions) between the two days of the case studies, this study presents the first work documenting observational results that are consistent with theoretical predictions for the dependence of the latitude distribution of the precipitation regions on the *L*-shells at which the nonducted whistler wave energy is released.

[28] On the two days we study, the VLF data was acquired at different receivers of the HAIL array. On the first day, 24 March 2001, five receivers were operating, located at Fort Collins (FC), Boulder (BD), Colorado Springs (CS), and Walsenburg (WS), Colorado, and Cheyenne, Wyoming (CH). On the second day, 28 March 2001, receivers at six HAIL sites were operational, located at Boulder, Littleton (LT), Parker (PK), Colorado Springs, and Walsenburg, Colorado along with Las Vegas, New Mexico (LV). All of these receivers are components of the overall HAIL array and monitor the amplitudes of both the NAA and NAU transmitter signals as well as other signals (arriving from the west).

3.1. Case 1: 24 March 2001

[29] Between 6:00 and 10:00 UT, HAIL data from multiple receivers exhibited VLF signatures of numerous LEP events on both the NAA and NAU transmitters. In those four hours, 80 LEP events with a maximum perturbation of at least 0.5 dB were recorded. All events were detectable on at least three sets of VLF paths.

[30] A typical LEP event for the time period is shown in Figure 7. The top panel shows a 3-min sequence of HAIL data, exhibiting a large signal perturbation meeting the criteria of the LEP event classification. The event marked at ∼7:13:20 UT is clearly visible on multiple paths, which are displayed on the map below. The distance ($\Delta\lambda_m$), in degrees latitude, between the flash location and the point of crossing of the GCP of the geomagnetic longitude of the causative flash is shown for each signal. Each perturbed signal is a separate data set for analysis, yielding measurements of onset delay, event duration, perturbation size, and recovery time versus this distance. For this event, a lightning flash in northern Texas causes precipitation in a region poleward displaced with respect to the location of the causative lightning, and a hypothetical map of the precipitation region (taken from *Lauben et al.* [1999]) is superimposed on the map. A perturbation is observed on the paths denoted by dashed lines, but no measurable perturbation was detected on the paths denoted by solid lines. The southernmost paths (NAU-CS and NAU-WS) and the northernmost path (NAA-CH) do not exhibit any perturbation, meaning the full latitudinal extent of the LEP precipitation region was captured. The majority of the LEP events

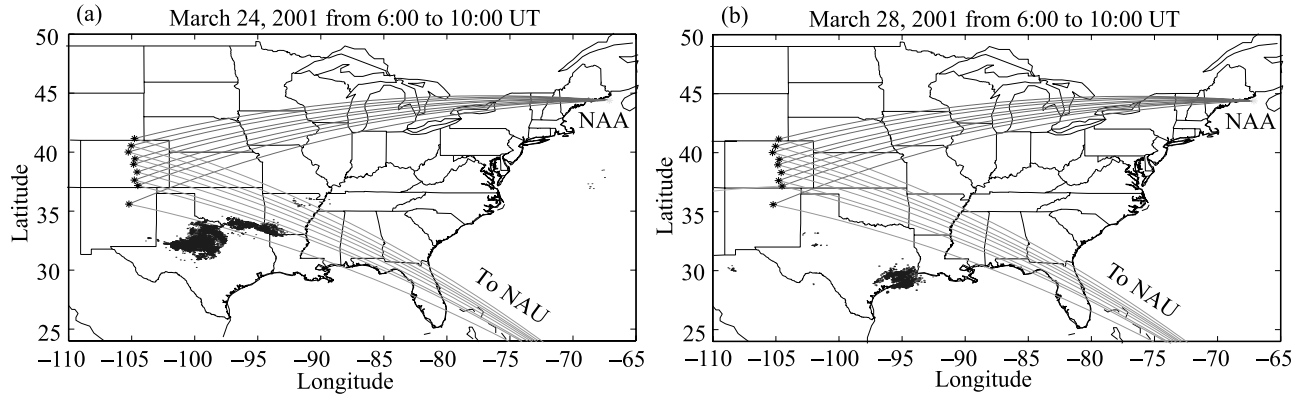

Figure 6. The location of all CG discharges recorded by NLDN from 6:00 to 10:00 UT on (a) 24 March and (b) 28 March 2001.

during this time period were detected in a similar location, with multiple paths perturbed and the full spatial extent of the event captured with the available VLF signal paths.

3.2. Case 2: 28 March 2001

[31] Similarly, HAIL data exhibited multiple VLF signatures of LEP events on both the NAA and NAU transmitters between 6:00 and 10:00 UT on 28 March 2001. Over the 4-hour period, 81 LEP events with perturbations of at least 0.5 dB were recorded. Figure 8 illustrates an example of one such event. A large LEP event at ~6:42:07 UT is recorded in the top panel, with the theoretical precipitation region superimposed on the map below. While different stations were recording data during this day, the event is once again observable on only some of the paths (denoted by dashed lines), while there are no discernible perturbations on other paths (denoted by solid lines). The causative discharge was located on the southeastern coast of Texas, and therefore the region of precipitation is expected to be centered at a different latitude than on 24 March. It should also be noted that the southernmost (NAU-LV) and northernmost paths (NAA-PK, NAA-CS) do not exhibit any VLF perturbation, indicating that the latitudinal extent of the LEP precipitation region was once again captured.

4. Temporal Features of VLF Signatures of LEP Events

[32] The VLF signatures of the LEP events monitored during these two days were time-correlated with CG lightning flashes recorded in the NLDN data, and the previously defined measurable temporal and spatial features were determined. A statistical analysis of these parameters is presented in this section.

4.1. Cloud-to-Ground (CG) Lightning

[33] For each LEP event included in this study, a sferic (an impulse in the received signal) associated with the causative lightning discharge was measured at many of the HAIL sites with 10 ms resolution. The recorded timing of the sferic was then associated with a CG discharge in the high resolution (1 ms) NLDN data. The majority of the causative flashes had both discernible sferics associated with the causative lightning flash and a corresponding CG discharge in the NLDN data (typically within measurement resolution, or 10 ms of the causative sferic time). Of the 80 events on 24 March, 72 (or 90%) were time-coincident with a CG flash in the NLDN data. On 28 March, 68 of 81 (or 84%) events were time-coincident with CG discharges. Though intracloud (IC) lightning is generally more common than CG flashes at these latitudes [*Prentice and Mackeras*, 1971], the NLDN network typically does not record them. By design, the NLDN network records only CG lightning flashes, with a detection efficiency of between 80% and 90% at these locations [*Cummins et al.*, 1998]. The fact that over 80% of the LEP events were time-coincident with CG flashes in the NLDN data implies that CG flashes induced nearly all of the detected LEP events (i.e., those events for which there are no associated NLDN recorded flashes were probably simply missed by the NLDN). The potential role of IC discharges will remain undetermined until there is a reliable method of recording them. In this connection, it should be noted that while VLF recordings at HAIL sites routinely record impulsive sferics from both CG and IC flashes, there is no easy way by which the flash type or location can be determined from this data. Previous work [*Inan et al.*, 1988a], also associated the majority of LEP events with CG discharges, but the lower detection efficiency of the lightning detection network in the region of that particular case study (the storm was substantially away from the coast) prevented the association of as high a percentage of LEP events with CG lightning discharges.

[34] Figures 9a–9c and Figures 10a–10c show that the majority of CG flashes detected by the NLDN network (all occurring within the same two storms) did not produce perturbations on the HAIL array consistent with our criteria for LEP events. During the 4-hour period on 24 March, only 80 of the 34,725 detected CG flashes (0.23%) produced LEP events with perturbations greater than 0.5 dB. Similarly, only 81 of 4,810 flashes (1.68%) produced LEP events with perturbations greater than 0.5 dB during the period analyzed on 28 March. Figures 9c and 10c show that a larger percentage (up to ~30%) of lightning discharges with higher peak current magnitudes (>100 kA) produced detectable LEP events, although even the largest flashes are not sure to be associated with LEP events. The polarity of the peak current signifies the direction the charge flow (from cloud-to-ground or ground-to-cloud). Both of these

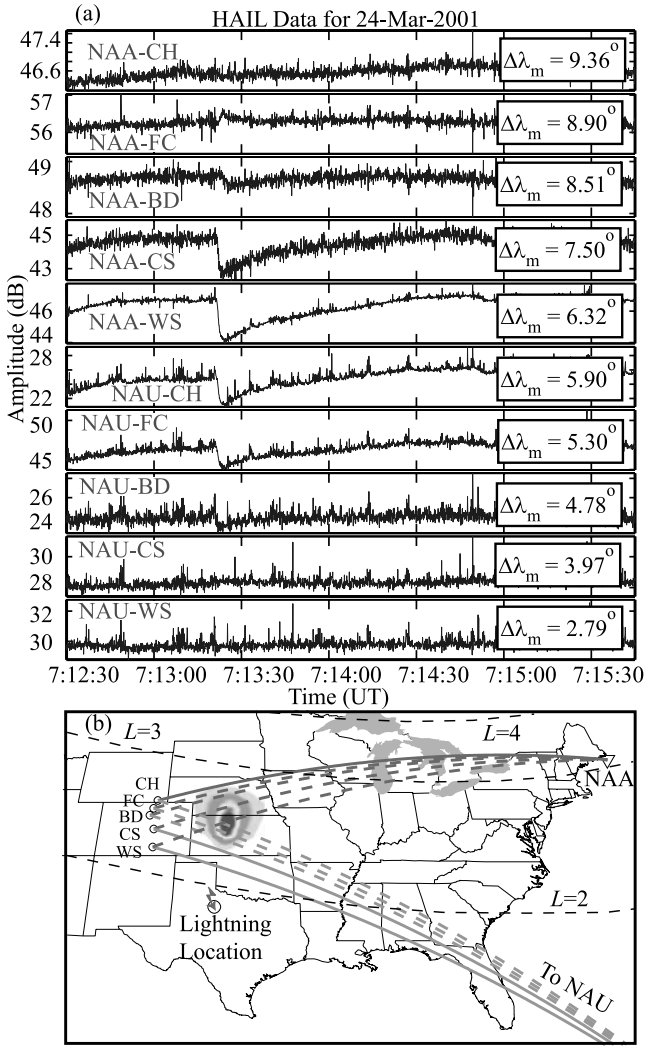

Figure 7. Typical LEP event observed on 24 March 2001. (a) A 3-min record of the amplitude (in dB) received at the five HAIL sites. The distance ($\Delta\lambda_m$), in degrees latitude, between the flash location and the point of crossing of the GCP of the geomagnectic longitude of the causative flash is shown for each signal. (b) The map shows the location of the HAIL sites, together with GCPs from the two VLF transmitters. Footprints of the $L = 2$ and $L = 3$ field lines are shown for reference. The causative lightning (7:13:20.723) was located in northern Texas (35°41′N, 92°4′W). The inferred region of precipitation is superimposed on the map. An associated VLF perturbation was detected on signals arriving along those great circle paths denoted by dashed lines, with no measurable perturbation detected on signals propagating along the paths denoted by solid lines.

polarities are referred to as CG discharges here. The data in hand does not suggest any dependence on the polarity of the current, but rather only on its magnitude. Such a dependence is expected since the LEP event is believed to be produced by the electromagnetic impulse generated by the lightning discharge, which couples through the ionosphere and the magnetosphere and becomes a whistler, and both positive and negative flashes can equally generate such electromagnetic waves, the magnitude of which is only determined by the rate of change of current [*Uman*, 1984, p. 61]. Discharges with larger peak currents produce more electromagnetic radiation, and therefore release more wave energy into the magnetosphere that can propagate as a nonducted whistler and induce electron precipitation.

[35] While previous studies of LEP events produced by ducted whistlers noted the presence of the magnetospheric duct as a necessary condition for the occurrence of an LEP event, no such condition is required for the occurrence of nonducted LEP events. There is no reason not to expect that smaller discharges also cause LEP events, but the wave energy released by these lower currents may not produce enough wave-induced precipitation and associated second-

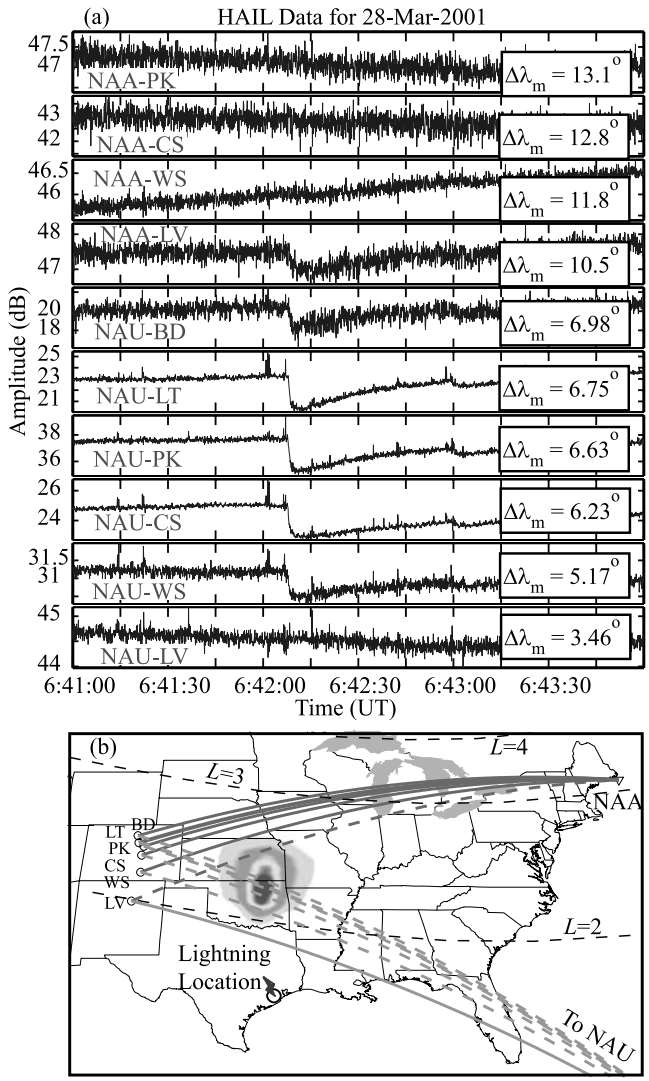

Figure 8. Typical LEP events observed on 28 March 2001. (a) A 3-min record of the received amplitude (in dB) at the six operating HAIL sites. The distance ($\Delta\lambda_m$), in degrees latitude, between the flash location and the point of crossing of the GCP of the geomagnectic longitude of the causative flash is shown for each signal. (b) The causative lightning (6:42:07.023 UT) was located on the southeastern coast of Texas (29°19′N, 95°28′W). The inferred region of precipitation is superimposed. The format of the figure is identical to that of Figure 7.

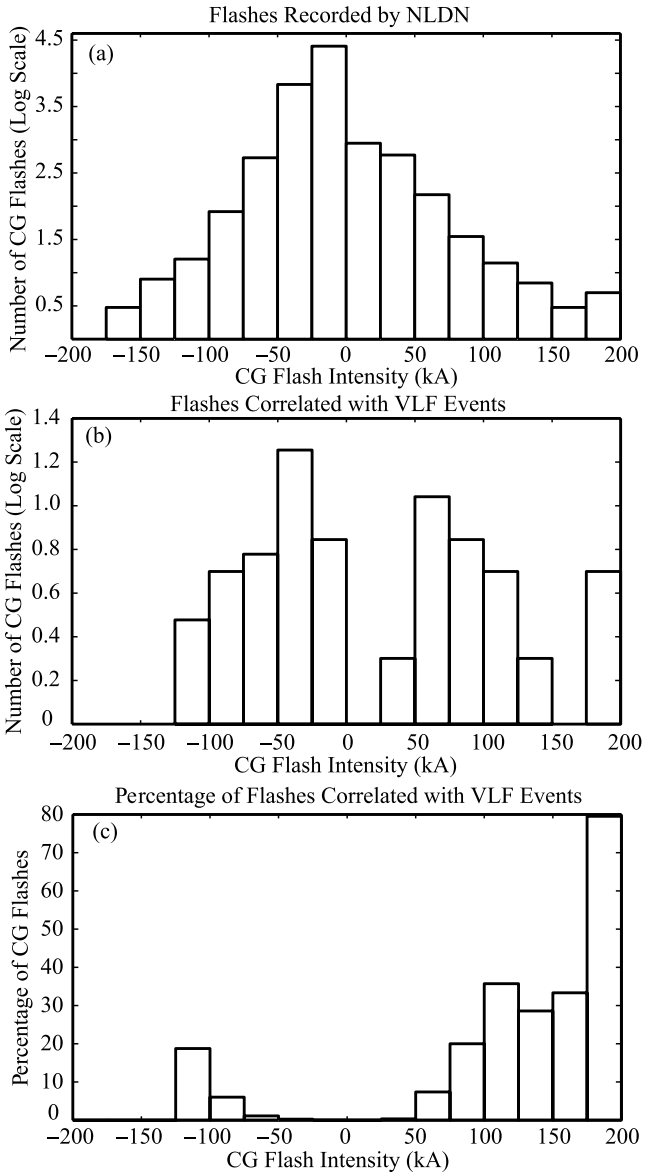

Figure 9. (a) Distribution (shown on a log scale) of all CG flashes detected by the NLDN network in terms of flash intensity for the period from 06:00 to 10:00 UT on 24 March 2001. (b) The distribution of CG flashes (shown on a log scale) time-correlated with VLF LEP events in terms of flash intensity for the same period. (c) Percentages of all CG flashes detected by the NLDN network that are time-correlated with VLF LEP events, in terms of CG flash intensity. As for all histograms following, those bins with three or less data points were deemed to not be statistically significant, and thus not shown.

ary ionization to which the subionospheric VLF signals can measurably respond.

[36] Lightning flashes occurring in the northern hemisphere, such as those studied here, produce south-going whistler waves, causing counter-streaming resonant particles perturbed through gyroresonance interaction with the south-going whistler wave to precipitate into the northern hemisphere. This type of precipitation is referred to as "direct" precipitation, as opposed to "mirrored" precipitation [*Inan et al.*, 1985, 1988a]. Particles are also precipitated in the southern hemisphere ("mirrored" precipitation) as a result of gyroresonance interaction with south-going whistler waves after first mirroring and/or backscattering in the north. At the geographic longitudes of the regions studied in this paper, the magnetic field at 100 km altitude is stronger in the northern hemisphere, and thus the mirror height for trapped energetic electrons is higher, than in the conjugate point in the southern hemisphere. Therefore if electrons just

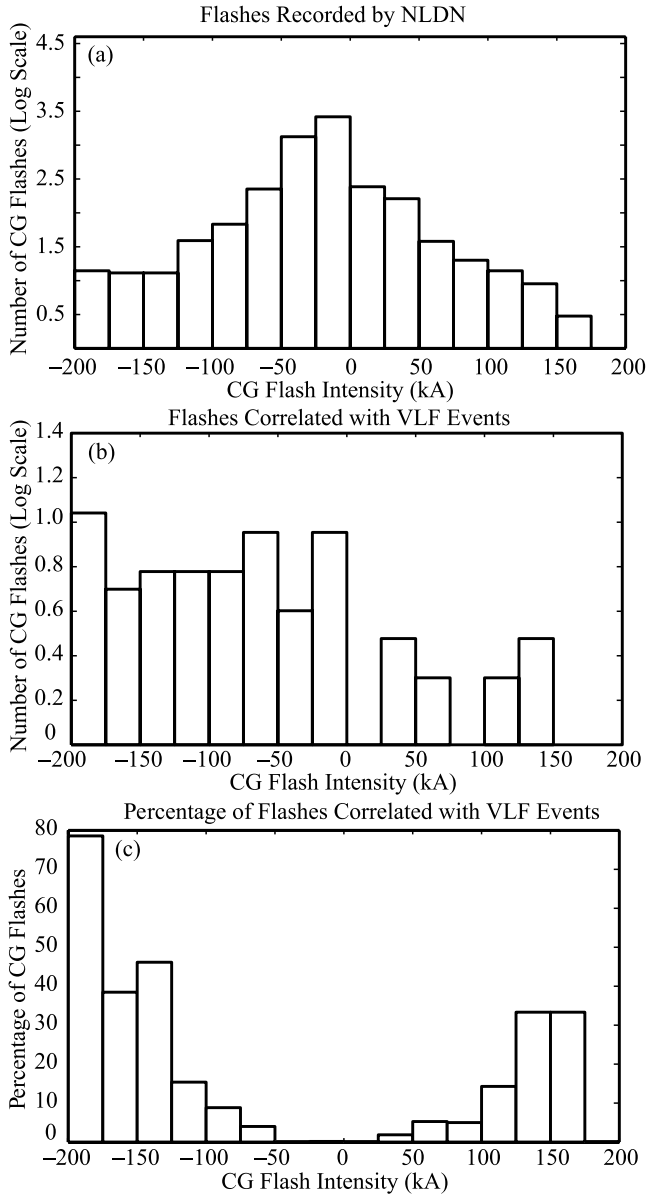

Figure 10. (a) Distribution (shown on a log scale) of all CG flashes detected by the NLDN network in terms of flash intensity for the period from 6:00 to 10:00 UT on 28 March 2001. (b) The distribution of CG flashes (shown on a log scale) time-correlated with VLF LEP events in terms of flash intensity for the same period. (c) Percentages of all CG flashes detected by the NLDN network that are time-correlated with VLF LEP events, in terms of CG flash intensity.

above the loss cone are weakly scattered into the loss cone, they do not all precipitate into the atmosphere in the northern hemisphere but rather mirror and backscatter and return to the southern hemisphere where they are deposited into the upper atmosphere. Only in cases when the pitch angle scattering is sufficiently strong would a burst of electrons precipitate the atmosphere in the north. For causative lightning flashes located near the conjugate of the South Atlantic magnetic anomaly, as is the case here, mirrored precipitation is thus believed to be significantly more effective (i.e., higher precipitated flux levels are expected) than direct precipitation [*Inan et al.*, 1988b]. This circumstance is one possible reason that the majority of CG flashes detected by the NLDN network did not produce detectable precipitation on the HAIL array. This observation also suggests that higher precipitated flux levels (and thus a higher number of precipitation events above a threshold) could be expected in the southern hemisphere, and that measurements of precipitation in the northern hemisphere may represent only a small fraction of the total amount of energetic electrons that are precipitated into the atmosphere and lost from the radiation belts.

[37] In summary, there are multiple reasons for the low percentage of CG discharges in the NLDN data that are time-correlated with LEP events. Firstly, only events with perturbation magnitudes greater than 0.5 dB are considered here. Secondly, the ''direct'' precipitation measured at the longitudes of the HAIL array, is expected to be less pronounced than the ''mirrored'' precipitation induced in the southern hemisphere, due to the South Atlantic anomaly. These two factors imply that in our study we observe events due to only those whistlers that cause the strongest pitch angle scattering of electrons, and thus the most intense precipitation bursts, while the majority of the induced precipitation may be below the threshold of observation. Finally, other factors, such as magnetospheric effects and the properties of the CG discharges, may influence the amount of induced precipitation.

[38] The variability and low efficiency of CG flashes in producing detected LEP events leads us to recommend that further study is needed to determine what is missing in the theoretical descriptions of this process. Simultaneous observations of precipitation in both hemispheres have been carried out in a few selected cases [e.g., *Burgess and Inan*, 1990], and future studies will be directed towards quantifying the relative amounts of precipitation in the northern and southern hemispheres. Establishing such a relationship is beyond the scope of this paper. Previous work [e.g., *Bortnik et al.*, 2003; *Abel and Thorne*, 1998a, 1998b] has suggested wave energy injected by lightning discharges may be an important contributor to the loss rates of radiation belt particles, especially at lower L-shells ($L < 3$), demonstrating the need for further studies on the properties of lightning discharges and geomagnetic conditions that influence LEP event activity.

4.2. Temporal and Spatial Characteristics of LEP Events

[39] The four measurables: event perturbation magnitude, onset delay, event duration and recovery time, were recorded for each LEP event. While this study constitutes the first statistical work aimed at quantifying these parameters, there have been several previous theoretical and experimental works on individual events. In this context, our statistical results are compared to both results of past experimental work [*Johnson et al.*, 1999] and theoretical predictions [*Lauben et al.*, 2001].

[40] The theoretical predictions of *Lauben et al.* [1999, 2001] are based on a quantitative model of oblique whistler-induced electron precipitation. This model predicts the temporal and spatial characteristics of ionospheric disturbances caused by lightning discharges occurring at mid-latitudes. A simple tilted dipole magnetic field model with typical magnetospheric conditions was modeled, with peak currents of the lightning discharges at 10 kA, generally lower than those discharges that were associated with LEP events in this study. *Johnson et al.* [1999] reported on a number of LEP events monitored on 18 October 1998, with the causative discharges located in the middle of Texas. In that work, no attempt was made to correlate the event measurables with the location of the causative discharges, so the influence the latitude of the causative discharge had on the LEP event signatures was not considered.

[41] Only those LEP events successfully correlated with CG discharges in the NLDN data (72 events on 24 March, 68 events on 28 March) were included in the data analysis. For each of these events the geomagnetic latitude and longitude of the causative lightning discharge were taken from the NLDN data. For each received signal, the intersection point of the great circle path (GCP) and the magnetic longitude of the causative discharge was calculated. The distance (in degrees of latitude and kilometers) between the location of the causative discharge and this intersection point was then calculated for each received signal. All data points were then binned according to this distance between the causative discharge and precipitation region location, and the values for each bin were averaged and plotted in histogram format. An uncertainty in latitude of $\pm 30'$ was introduced by the binning of the data sets, and this uncertainty includes the standard deviation (due to the distribution of data points as measured) and any observational error, which was generally on a smaller scale than the standard deviation. Throughout this paper, the use of the symbol $\pm$ is meant to signify the uncertainty of the measurement, including the standard deviation and/or observational errors.

4.2.1. Spatial Signatures of LEP Regions

[42] Figure 11 shows the magnitude of perturbation of the VLF signal versus the distance between the causative discharge and the corresponding location on the GCP. As mentioned previously, the HAIL array captures the peak and latitudinal extent of the precipitation regions on both days. Due to the disposition of the array, only variations in latitude are distinguishable, and for the purposes of this study, we assume the precipitation region to be longitudinally symmetric. Such an assumption is consistent with previous predictions [*Lauben et al.*, 1999] based on a simple tilted dipole model and neglecting longitudinal gradients in the Earth's magnetic field or cold plasma density.

[43] On 24 March, the mean location of all CG flashes detected by the NLDN network for the four-hour period between 6:00 and 10:00 UT was at $32°57'$N latitude. Figure 11a shows that the measured peak of the perturbation occurred in the $6°30'$ to $7°$ (715 to 770 km) bin north of

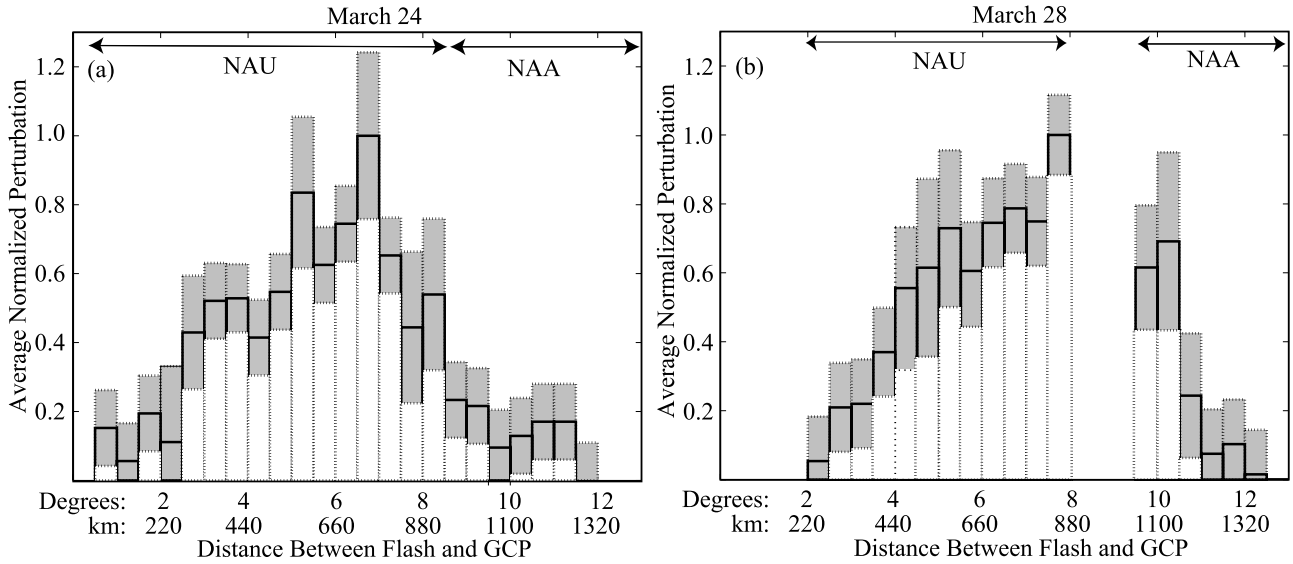

Figure 11. The normalized magnitude of perturbations caused by LEP events as a function of distance between the flash location and great circle path (GCP) for 24 March (a) and 28 March (b) 2001. All values were first binned (bins demarcated by dashed lines) according to the distance between flash location and the point of crossing of the GCP of the geomagnetic longitude of the causative flash, and all values in each bin were subsequently averaged (shown by a solid line). The standard deviation incorporates the measurement error and is denoted by the shaded area. The measurements taken from the more northern NAA paths and the more southern NAU paths are denoted as such. The gap in data on 28 March is due to the gap between the NAA and NAU GCPs (see Figure 8). The normalization was done separately for the measurements taken on NAA and NAU signals, due to their different sensitivities to a given perturbation, and noting the frequency difference and great circle path differences between these two signals. Normalization was performed to realize continuity between the two measurements, and bring any overlapping measurements into agreement. Distance is in both degrees latitude and kilometers.

this, at 39°42′ ± 30′N. The majority (>90%) of the precipitation occurs in the region 2° ± 30′ to 10° ± 30′ poleward of the causative discharge, over a range of 880 ± 110 km. A similar precipitation pattern is measured on 28 March. The mean location for the CG discharges detected by the NLDN network between 6:00 and 10:00 UT is located further south (29°9′N), and the nonducted wave energy is injected at a slightly lower *L*-shell. The gap in the data, from 8° to 9°, is due to the lack of overlap between the NAA and NAU GCPs for this location. Despite a shape similar to that on 24 March, the peak is displaced further, in the 7°30′ to 8° (825 to 880 km) bin north of the causative thunderstorm, at a corresponding latitude of 36°50′ ± 30′N. The majority (90%) of the precipitation occurs in a region 3° ± 30′ to 12° ± 30′ poleward of the causative discharge, over a range of 990 ± 110 km, more extensive than that on 24 March. Therefore those events associated with causative discharges at lower latitudes (those on 28 March), typically exhibit a larger region of precipitation and are displaced further poleward from the causative discharge.

[44] When compared to the theoretical predictions for nonducted whistler-induced precipitation, our results agree well with the general spatial disposition of the precipitation region. Figure 12 shows *Lauben et al.* [2001] model predictions for the longitude- and time-integrated precipitation energy flux profile, for energy ranges E > 100 keV, due to a 10 kA peak current discharge with a lightning source latitude (29°N) comparable to those of the case studies. The solid black line depicts the theoretical values obtained from the model, with the peak of precipitation denoted by the solid arrow. The energy flux is plotted on a log scale as a function of distance between the flash location and the point of precipitation, the same horizontal axis as that for Figure 11.

[45] A third-order polynomial was fit to the measured perturbation magnitude (Figure 11) for both days studied herein, with a correlation coefficient of 0.84 for 24 March and 0.91 for 28 March. *Inan and Carpenter* [1987] showed that for single-waveguide mode propagation the change of amplitude in the VLF signal (ΔA) is proportional to $d\Delta h$, with d being the extent of the perturbed region along the propagation path and Δh being the differential reduction of the lower ionospheric reflection height for the VLF signal. Although VLF propagation on shorter paths (and on land) is more complicated and generally involves the superposition of several waveguide modes [e.g., *Poulsen et al.*, 1993a], we assume here that $d\Delta h$ is proportionally related to the change in the electron density, ΔN_e, and therefore to the precipitated energy flux density [*Poulsen et al.*, 1993a], in order to provide a basis for comparison of our measurements of event perturbation magnitude (ΔA) directly to the theoretical predictions of energy flux density presented in *Lauben et al.* [2001]. The measured values for perturbation magnitude (denoted by dashed lines) may be compared to the theoretical values for precipitation flux (Figure 11) obtained from the model (denoted by the solid curve). For the light (28 March) and dark (24 March) dashed lines, the peaks are denoted by the dashed arrows and the peak values are normalized to match the peak value predicted by the model.

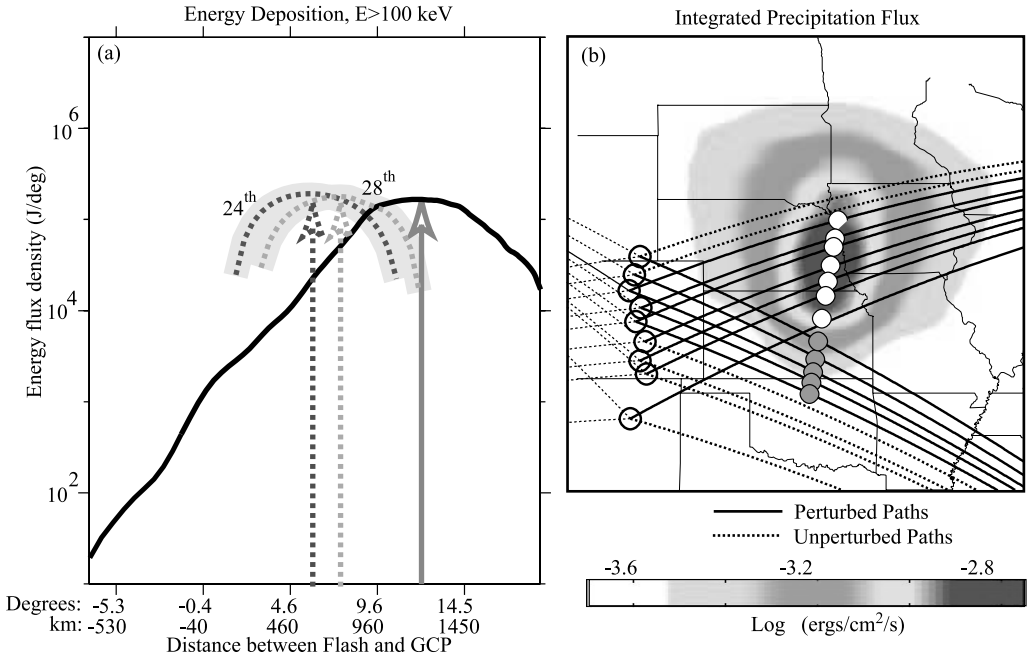

Figure 12. (a) The longitude- and time-integrated precipitation energy flux profile as a function of distance between the flash location and the great circle path (GCP), for energy ranges E > 100 keV and a lightning source latitude of ~29°N. The solid black line depicts the theoretical values obtained from the model, with the peak of precipitation denoted by the solid arrow. Third-order polynomials were fit to the normalized magnitude of perturbation measured on the two days (Figure 11), and represent the presumed energy flux density measured by the HAIL array based on the assumption that $\Delta A \propto \Delta N_e \propto Q(flux)$. The light (28 March) and dark (24 March) dashed lines denote the fitted polynomials, with the shaded areas denoting the observational uncertainty. The peaks are denoted by the dashed arrows, and are normalized to match the peak value predicted by the model. (b) The *Lauben et al.* [1999] model predictions of time-integrated precipitation flux for E > 100 keV due to a 10 kA peak current discharge, superimposed on a map of the GCPs. Modified from *Lauben et al.* [2001] and *Johnson et al.* [1999].

[46] For lightning located at a similar latitude, the majority of the electron flux is predicted to be deposited at $L > 2$, at slightly higher latitudes than observed in the two case studies. The model predicts that the peak of the energy flux deposited would have a greater poleward displacement (12°) from the causative discharge than that observed (6°45′ ± 30′ on 24 March and 7°45′ ± 30′ on 28 March). Over 90% of the precipitation occurs within a region of 880 ± 110 km (8° ± 1°) on 24 March, and 990 ± 110 km (9° ± 1°) on 28 March. This is a smaller region than that predicted by the model (1380 ± 110 km or 12°30′ ± 1°), especially considering the fact that the causative discharges typically had larger peak currents than those used in the model (10 kA). This smaller precipitation region may be a result of the *L*-shell dependence of the flux of trapped energetic electrons, which was assumed uniform in *Lauben et al.* [1999, 2001]. Another possible explanation is that the smaller precipitation region is a result of differences in the relative amounts of "direct" versus "mirrored" precipitation induced, as discussed in section 4.1, which was not considered with the simple titled dipole field model used in *Lauben et al.* [1999, 2001].

[47] The *Lauben et al.* [1999, 2001] model predicts a larger region of precipitation for causative discharges located at lower latitudes. The same qualitative trend is seen in the observed data for the two periods of the case study, with larger regions of precipitation associated with causative discharges located at lower latitudes (28 March) than higher latitudes (24 March). The previous experimental measurements [e.g., *Johnson et al.*, 1999, Figure 4] were similar to the perturbation signatures observed here, both qualitatively and quantitatively.

[48] In terms of the poleward displacement of the precipitation region, the *Lauben et al.* [1999, 2001] model predicts that the precipitation region would have a greater poleward displacement (with respect to its causative discharge) for source lightning located at lower latitudes. This prediction is consistent with the larger poleward displacement observed on 28 March than on 24 March, although the absolute value of the poleward displacement predicted by the model is larger than either of those observed on the 2 days.

[49] These discrepancies may indicate that the actual oblique whistler-mode raypaths may have been confined to lower *L*-shells than those in the model, due to a more rapid radial variation of the magnetospheric cold plasma density. The *Lauben et al.* [2001] model used a static geomagnetic dipole field model, while the observations were recorded during two highly active geomagnetic periods (Figures 4 and 5). However, the differences in geomagnetic conditions for the two days of the case study are unlikely to change the location of the *L*-shell footprints significantly at these latitudes, and so the differences

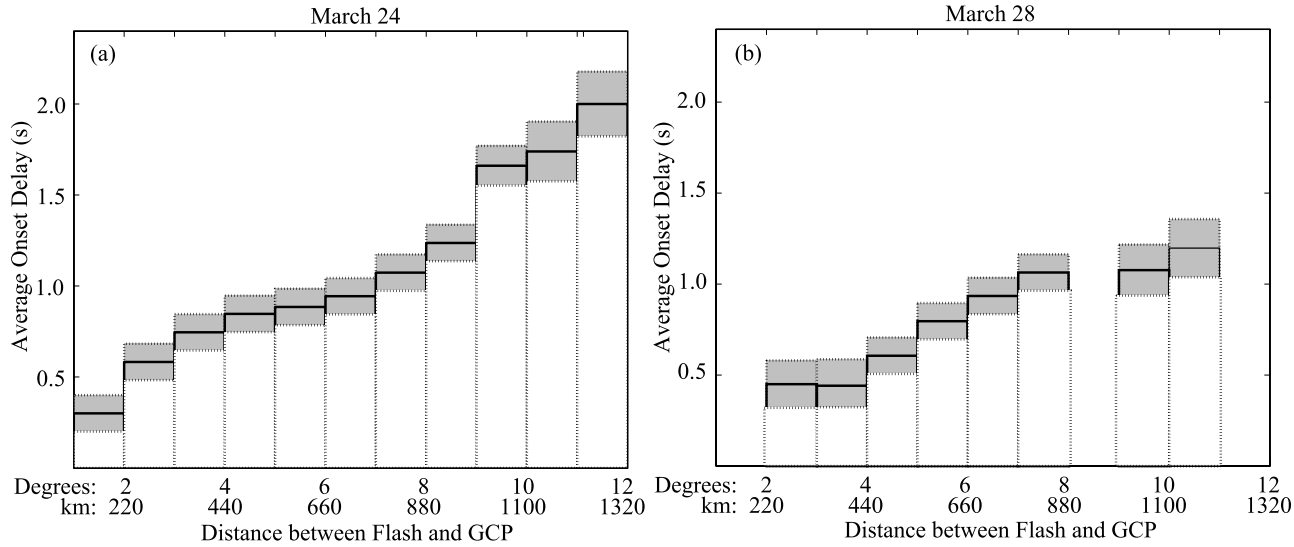

Figure 13. Average onset delay for the LEP events as a function of distance between flash location and great circle path (GCP) for 24 March (a) and 28 March (b) 2001. All values were first binned according to the distance from the flash, and then averaged (shown by a solid line). The standard deviation incorporates measurement error and is denoted by the shaded area. Distance is in both degrees latitude and kilometers.

observed between the two case studies are not likely to be due to the compression of the inner magnetosphere. We note that the latitudinal displacement observed on the two days is more in line with that measured in *Johnson et al.* [1999].

[50] In summary, while past experimental work coincides with our results quantitatively, the theoretical model predicts slightly larger displacements and wider precipitation regions than those observed. The differences in the poleward displacement and the size of the perturbation region for causative discharges of different latitudes agree with theoretical predictions. However, it is possible that variations in geomagnetic conditions (especially the equatorial profile of the cold plasma density) may influence the spatial properties of the precipitation region. A study of simultaneous LEP events occurring at widely different *L*-shells is needed to account for the relation of such variability to magnetospheric effects.

4.2.2. Onset Delay

[51] Figure 13 shows the average onset delay versus the distance between the causative discharge and the corresponding disturbance point along the GCP. The measurements are first binned according to their distance from the causative discharge, and the values in each bin are subsequently averaged to determine a mean and standard deviation for each bin. A linear increase in onset delay with latitude is evident for both days. The onset delay and distance from the lightning source are related with a correlation coefficient of 0.97 on 24 March and 0.96 on 28 March. This correlation means that the onset of precipitation is delayed proportionally to the northward displacement from the causative discharge. On 24 March, events are generally first observed 0.3 ± 0.1 s after the causative discharge, and thereafter extend northward in latitude, with the most northern paths perturbed 2.0 ± 0.2 s after the original discharge. The onset delay increases 0.15 ± 0.05 s per degree in latitude ($1.4 \pm 0.5 \times 10^{-3}$ s/km). On 28 March, the events are first seen 0.4 ± 0.2 s after the causative discharge and again extend northward in latitude, with the northernmost paths perturbed 1.2 ± 0.2 s after the discharge. The event is seen to extend northward at a slower rate than on 24 March, with the onset delay increasing 0.08 ± 0.04 s per degree ($7.3 \pm 0.4 \times 10^{-4}$ s/km). Therefore, for those events associated with causative discharges located at lower latitudes (28 March), the onset delay increases less rapidly with increasing latitude.

[52] The nearly linear increase in onset delay with increasing *L*-value is consistent with both the previous experimental and theoretical works. Figure 15 shows an overlay of individual precipitation energy flux profiles for selected *L* shells based on theoretical predictions from *Lauben et al.* [2001]. Only some of the curves ($2.4 < L < 3$) are relevant at these latitudes. The onset delays predicted by the model (0.2 s to 0.8 s) were shorter than those observed here, indicating that the magnetospheric cold plasma density values used in the model were lower than those present during our measurements. The events monitored during October 1998 [*Johnson et al.*, 1999] are more in line with those measured here. The differences between the two case studies in the rate of increase in onset delay with latitude are not easily explained by the model, and may be due to differences in magnetospheric conditions, such as differences in the cold plasma density profile as a function of *L*-shell (which determines the wave and particle travel times to and from the interaction regions and thus the onset delay). The sensitivity of electron precipitation to magnetospheric conditions (e.g., the cold plasma density) suggests the possible use of the measured temporal and spatial signatures of LEP events as a means of remote sensing the variation of cold plasma density in the magnetosphere.

4.2.3. Event Duration

[53] The format of Figure 14 is identical to that of Figure 13, except that the event duration is plotted rather than the onset delay. Once again, a linear increase with increasing *L*-shell is evident on both days. The event

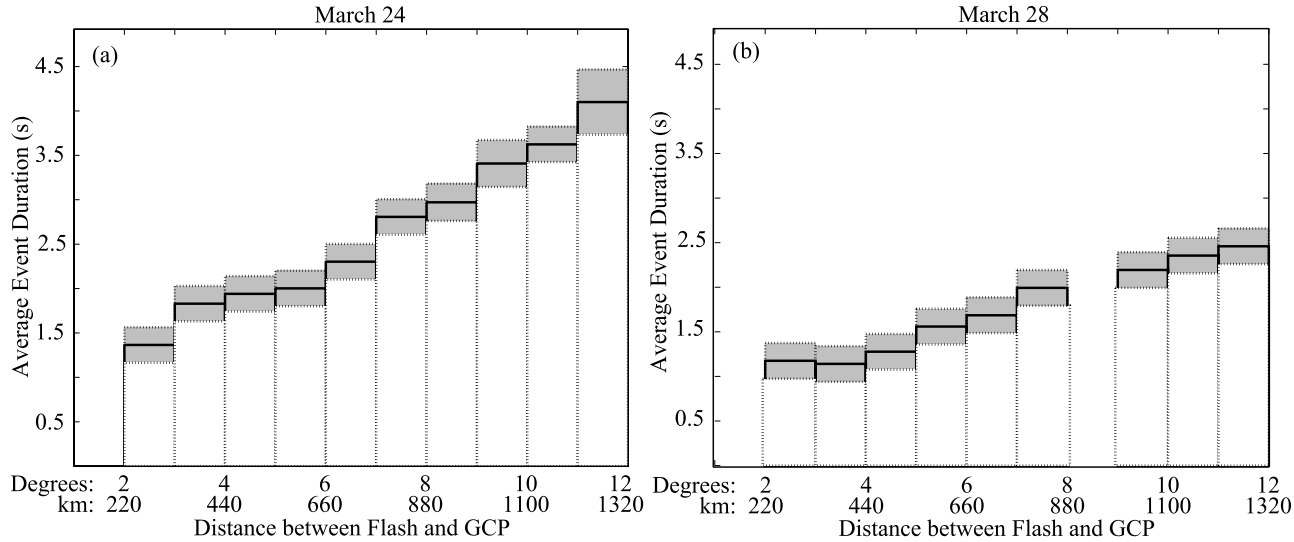

Figure 14. Average event duration for the LEP events as a function of distance between flash location and great circle path (GCP) for 24 March (a) and 28 March (b). The format is identical to that of Figure 13, with the average value for each bin denoted by a solid line and the standard deviation denoted by the shaded area.

duration and distance from the lightning source are related with a correlation coefficient of 0.98 on 24 March and 0.91 on 28 March. This means that the further north from the causative discharge, the later the precipitation begins, but also that the precipitation persists longer. On 24 March, the duration increases from 1.5 ± 0.2 s at the most southern measurement to 4.1 ± 0.5 s at the most northern. This gives a rate of increase in duration of 0.26 ± 0.07 s per degree latitude ($2.3 \pm 0.6 \times 10^{-3}$ s/km). For 28 March, the duration increases from 1.2 ± 0.2 to 2.5 ± 0.2 s; the precipitation does not continue as long as on 24 March. The rate of increase on 28 March is less than on 24 March, at 0.13 ± 0.04 s per degree ($1.2 \pm 0.4 \times 10^{-3}$ s/km). To summarize, those events associated with causative discharges at lower latitudes (those on 28 March), generally exhibit shorter durations and a slower rate of increase in duration with latitude.

[54] The increase in duration with increasing L-value is predicted by the theoretical model (Figure 15). The model predicts shorter durations (0.3 to 1.0 s) at lower latitudes (L-shells), with significantly longer durations (0.5 to 1.4 s) at higher latitudes, more similar to those of the case studies. The generally shorter durations predicted by the model may be indicative of a lower than usual cold plasma density in the magnetosphere, which would result in increased propagation speeds for the wave and also higher energies (and thus faster travel times) for resonant electrons. It should also be noted that the model does not include magnetospheric reflections of the obliquely propagating whistler-mode wave, which have been recently shown to lengthen the duration of electron precipitation [*Bortnik et al.*, 2003]. The differences between the 2 days analyzed here are not easily explained by the model, and may be due to differences in magnetospheric conditions, such as the cold plasma density profile, rather than due to a dependence of event duration on source latitude.

4.2.4. Event Recovery

[55] Finally, Figure 16 shows recovery time versus the distance between the causative discharge and the GCP. Conversely to the other spatial and temporal signatures, the recovery time showed no correlation to the distance from the source lightning, with an absolute correlation coefficient less than 0.4 for both days. This result is not unexpected, since the recovery time is not strongly dependent on the propagation characteristics of the nonducted whistler wave energy or other magnetospheric conditions. Recovery time is essentially the chemical response of the ionosphere to the newly introduced secondary ionization [*Pasko and Inan*, 1994] and is only dependent on the conditions of the ionosphere and the energy spectrum of the precipitating electrons (which then determines the altitude at which the secondary ionization is produced). The relatively slow recovery times are consistent with

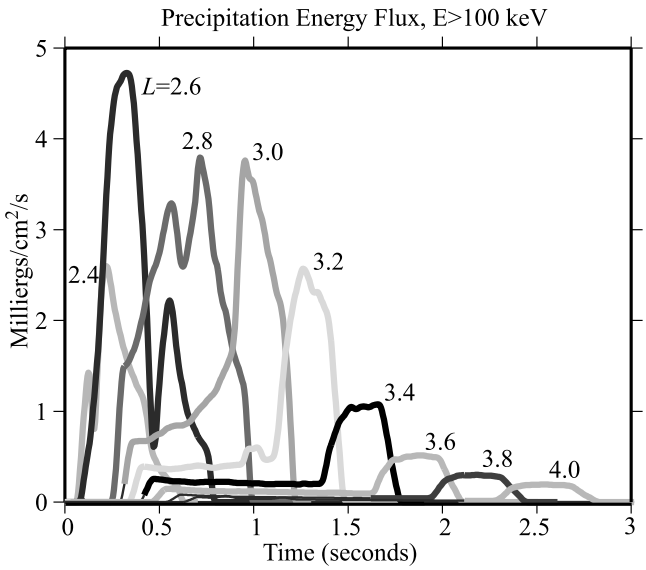

Figure 15. Overlay of the theoretical precipitation energy flux profiles evaluated for selected L shells spanning $1.8 < L < 4.0$ in the central meridian. Modified from *Lauben et al.* [2001].

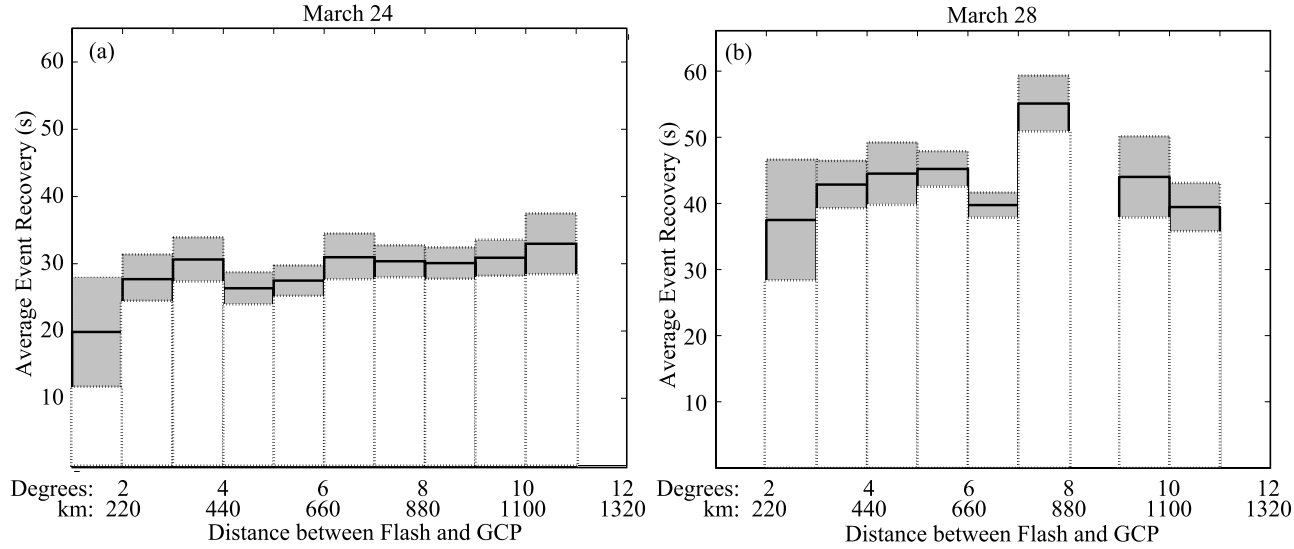

Figure 16. Average event recovery time for the LEP events as a function of distance between flash location and great circle path (GCP) for 24 March (a) and 28 March (b). The format is the same as Figures 13 and 14.

expected relaxation times for secondary ionization produced in the *D* region [*Glukhov et al.*, 1992]. While the recovery time is nearly constant across the array, it is different on the 2 days of the study, with a mean value and standard deviation of 28.7 and 4.2 s on 24 March, 41.1 and 8.6 s on 28 March, respectively. The differences in recovery time on the 2 days is probably a result of the energy spectrum of precipitation flux, which is determined (to a large degree) by the energy spectrum of the available trapped flux, known to be variable from day to day [*Demirkol et al.*, 1999].

5. Summary

[56] This first statistical analysis of the perturbations of VLF signals caused by nonducted whistler-induced electron precipitation yielded a quantification of temporal and spatial signatures of LEP events. The events were typified by a linear increase in onset delay and duration with increasing *L*-shell, while the recovery time was independent of latitude at these scales. The latitudinal variation of onset delay agreed with previous observations presented in *Johnson et al.* [1999]. The two case studies presented here concern storms located at different latitudes. For the case where causative discharges were located at lower latitudes, the LEP events exhibited shorter durations with less rapidly increasing onset delays and durations with latitude. They also exhibited precipitation in a wider area displaced further poleward from the causative discharge. The qualitative spatial and temporal characteristics were in general agreement with both previous measurements and theoretical predictions. A future study of simultaneous LEP events occurring at widely different *L*-shells is needed to more definitively determine the dependence of the temporal and spatial signatures of LEP events on the location of the causative discharge.

[57] **Acknowledgments.** This work was supported by the National Science Foundation and the Office of Naval Research under grants ATM-9910532 and N0094-00-1-0945. The authors thank the many high school teachers and students involved in the support of the HAIL array. We thank Robb Moore for his extensive field work and the use of his data acquisition software for the HAIL array. We thank Dr. Dave Evans of NOAA for the use of NOAA-POES data. We thank our colleagues in the STAR Laboratory for their useful commentary, and we also thank Dr. Ken Cummins of Vaisala for the use of NLDN data.

[58] Arthur Richmond thanks Bob Abel and J. Bernard Blake for their assistance in evaluating this paper.

References

Abel, B., and R. M. Thorne (1998a), Electron scattering loss in Earth's inner magnetosphere: 1. Dominant physical processes, *J. Geophys. Res.*, *103*, 2385–2396.

Abel, B., and R. M. Thorne (1998b), Electron scattering loss in Earth's inner magnetosphere: 2. Sensitivity to model parameters, *J. Geophys. Res.*, *103*, 2397–2407.

Bortnik, J., U. S. Inan, and T. F. Bell (2003), Energy distribution and lifetime of magnetospherically reflecting whistlers in the plasmasphere, *J. Geophys. Res.*, *108*(A5), 1199, doi:10.1029/2002JA009316.

Burgess, W. C., and U. S. Inan (1990), Simultaneous disturbance of conjugate ionospheric regions in association with individual lightning flashes, *Geophys. Res. Lett.*, *17*, 259–262.

Burgess, W. C., and U. S. Inan (1993), The role of ducted whistlers in the precipitation loss and equilibrium flux of radiation belt electrons, *J. Geophys. Res.*, *98*, 15,643–15,665.

Christian, H. F., et al. (1999), Global frequency and distribution of lightning as observed by the Optical Transient Detector (OTD), paper presented at 11th International Conference on Atmospheric Electricity, Global Hydrol. and Clim. Cent., Guntersville State Park, Ala., 7–11 June.

Cummins, K. L., M. J. Murphy, E. A. Bardo, W. L. Hiscox, R. B. Pyle, and A. E. Pifer (1998), A combined TOA/MDF technology upgrade of the U.S. National Lightning Detection Network, *J. Geophys. Res.*, *103*, 9035–9044.

Demirkol, M. K., U. S. Inan, T. F. Bell, S. G. Kanekal, and D. C. Wilkinson (1999), Ionospheric effects of relativistic electron enhancement events, *Geophys. Res. Lett.*, *26*, 3557–3560.

Friedel, R. H. W., and A. Korth (1995), Long-term observations of keV ion and electron variability in the outer radiation belt from CRRES, *Geophys. Res. Lett.*, *22*, 1853–1856.

Glukhov, V. S., V. P. Pasko, and U. S. Inan (1992), Relaxation of transient lower ionospheric disturbances caused by lightning-whistler-induced electron precipitation bursts, *J. Geophys. Res.*, *97*, 16,971–16,979.

Helliwell, R. A., J. P. Katsufrakis, and M. L. Trimpi (1973), Whistler-induced amplitude perturbation in VLF propagation, *J. Geophys. Res.*, *78*, 4679.

Inan, U. S., and D. L. Carpenter (1986), On the correlation of whistlers and associated subionospheric VLF/LF perturbations, *J. Geophys. Res.*, *91*, 3106.

Inan, U. S., and D. L. Carpenter (1987), Lightning-induced electron precipitation events observed at L ~ 2.4 as phase and amplitude perturbations on subionospheric VLF signals, *J. Geophys. Res.*, *92*, 3293–3303.

Inan, U. S., and J. V. Rodriguez (1993), Lightning-induced effects on VLF/LF radio propagation, in *ELF/VLF/LF Radio Propagation and System Aspects*, *AGARD-CP-529*, 9-1.

Inan, U. S., D. L. Carpenter, R. A. Helliwell, and J. P. Katsufrakis (1985), Subionospheric VLF/LF phase perturbations produced by lightning-whistler induced particle precipitation, *J. Geophys. Res.*, *90*, 7457.

Inan, U. S., D. C. Shafer, W. Y. Yip, and R. E. Orville (1988a), Subionospheric VLF signatures of nighttime *D* region perturbations in the vicinity of lightning discharges, *J. Geophys. Res.*, *93*, 11,455–11,472.

Inan, U. S., T. G. Wolf, and D. L. Carpenter (1988b), Geographic distribution of lightning-induced electron precipitation observed as VLF/LF perturbation events, *J. Geophys. Res.*, *93*, 9841.

Inan, U. S., T. F. Bell, V. P. Pasko, D. D. Sentman, E. M. Wescott, and W. A. Lyons (1995), VLF signatures of ionospheric disturbances associated with sprites, *Geophys. Res. Lett.*, *22*, 3461–3464.

Johnson, M. P., U. S. Inan, and D. S. Lauben (1999), Subionospheric VLF signatures of oblique (nonducted) whistler-induced precipitation, *Geophys. Res. Lett.*, *26*, 3569–3572.

Lauben, D. S., U. S. Inan, and T. F. Bell (1999), Poleward-displaced electron precipitation and lightning-generated oblique whistlers, *Geophys. Res. Lett.*, *26*, 2633–2636.

Lauben, D. S., U. S. Inan, and T. F. Bell (2001), Precipitation of radiation belt electrons induced by obliquely propagating lightning-generated whistlers, *J. Geophys. Res.*, *106*, 29,745–29,770.

Leyser, T. B., U. S. Inan, D. L. Carpenter, and M. L. Trimpi (1984), Diurnal variation of burst precipitation effects on subionospheric VLF/LF signal propagation near L = 2, *J. Geophys. Res.*, *89*, 9139–9143.

Pasko, V. P., and U. S. Inan (1994), Recovery signatures of lightning-associated VLF perturbation as a measure of the lower ionosphere, *J. Geophys. Res.*, *99*, 17,523–17,537.

Poulsen, W. L., U. S. Inan, and T. F. Bell (1993a), A multiple-mode three-dimensional model of VLF propagation in the Earth-ionosphere waveguide in the presence of localized *D* region disturbances, *J. Geophys. Res.*, *98*, 1705–1717.

Poulsen, W. L., T. F. Bell, and U. S. Inan (1993b), The scattering of VLF waves by localized ionospheric disturbances produced by lightning-induced electron precipitation, *J. Geophys. Res.*, *98*, 15,553–15,559.

Prentice, S. A., and D. Mackeras (1971), The ratio of cloud to cloud-ground lightning flashes in thunderstorms, *Radio Sci.*, *6*, 299.

Uman, M. A. (1984), *Lightning*, Dover, Mineola, N. Y.

Voss, H. D., M. Walt, W. L. Imhof, J. Mobilia, and U. S. Inan (1998), Satellite observations of lightning-induced electron precipitation, *J. Geophys. Res.*, *103*, 11,725–11,744.

U. S. Inan and W. B. Peter, STAR Laboratory, 351 Packard Bldg., Stanford, CA 94305, USA. (wpeter@stanford.edu)